Thermal treatment and environment effect on transient photoconductivity behavior of anatase TiO$_2$ with dominant {0 0 1} facets

K. Pomoni[a,*], T. Georgakopoulos[a], M.V. Sofianou[b], C. Trapalis[b]

[a]Department of Physics, University of Patras, 26504 Patras, Greece

[b]Institute of Advanced Materials, Physicochemical Processes, Nanotechnology and Microsystems, National Center for Scientific Research ''Demokritos'', 15310 Ag. Paraskevi Attikis, Greece

[*]K. Pomoni

Department of Physics, University of Patras, 26504 Patras, Greece

Tel.: +30 2610 997482

fax: +30 2610 997498.

E-mail address: pomoni@physics.upatras.gr

Abstract

Nanosized anatase TiO_2 powders with dominant {0 0 1} facets were prepared by solvothermal reaction of titanium isopropoxide in the presence of hydrofluoric acid as a capping agent. Two kinds of samples, as prepared and calcinated at 600 °C were fabricated and their UV–Visible and transient photoconductivity were investigated in vacuum and in air. The photoconductivity reaches high values and is sensitive on the environment. Thermal treatment improves the crystalline quality and enhances the amount of created excess charge carriers.

1. Introduction

In nature, TiO_2 has three different structures: brookite (orthorhombic), anatase (tetragonal) and rutile (tetragonal). Anatase TiO_2 is one of the most important semiconductors with many applications ranging from optics to gas sensors via solar energy [1] due to its high activity, chemical stability and nontoxicity [2, 3]. Modification of anatase properties owing to its electronic structure has been subject of intensive research [4-10].

The properties of TiO_2 are affected not only by the electronic structure but also by the size, the shape organization and surface properties [11, 12]. A commonly employed strategy to optimize the performance of various crystalline catalysts is the design and morphological control of their crystal facets [13]. Nanosheets are known as an important category of nanomaterials with a large surface area and an ultra thin thickness with many applications in nanodevices, photocatalysis, photoluminescence and battery materials [14]. TiO_2 nanosheets, among other sheet-like semiconducting

oxides nanomaterials, are attractive for their ultimate two-dimensionality with the thickness of subnano- to nanometer range, high crystallinity, well-defined composition and novel or enhanced physical properties [15]. Recently, layered TiO_2 with reactive {0 0 1} facets have shown excellent photocatalytic activity, resulting from the synergetic effects of the layered structure and the {0 0 1} facet-dominated nanosheets [16]. The physicochemical properties of TiO_2 are largely determined by the degree of exposure of the external surfaces [17]. The majority of the external surfaces of anatase $TiO2$ {1 0 1} unfortunately have a low reactivity originating from its low surface energy [18]. The anatase crystals are dominated by the less reactive {1 0 1} facets, since the crystal-growing process quickly diminishes the highly reactive {0 0 1} facets to minimize the surface energy [16]. Many efforts have been made to improve the percentage of highly reactive {0 0 1} facets (average surface energy 0.90 J m^{-2}) of anatase TiO_2 for the enhancement of its photocatalytic properties, making so this material attractive for environmental and energy related applications. Increasing research attention has focused on the controllable synthesis of anatase TiO^2 with exposed {0 0 1} facets, including traditional vaporphase epitaxial processes, hydrothermal/solvothermal methods, nonhydrolytic alcoholysis methods and high temperature gas phase reactions [18]. Since the total surface free-energy determines the shape, the general approach to control it is to grow the crystal in the presence of species that, binding with different adsorption energies to the different crystalline facets, affect their relative stabilities. Among species, the results indicate that a high percentage of anatase TiO^2 {0 0 1} facets is achieved if their surfaces are surrounded by F atoms [19-21]. More specifically, it is known from the literature that when the fluoride atoms are adsorbed on the {0 0 1} crystal facets the value of the (0 0 1) surface energy (γ) is lowered enhancing this way its formation during the crystallization

process. This effect is attributed to the low bonding energy (D_0) of F–F (158.8 kJ/mol) and the strong bonding energy of Ti–F (569.0 kJ/mol) [19,22]. Recently, a percentage of ~100% has been reached [23-26].

The photocatalytic mechanism is concerning to phenomena associated with photons absorption, charge-carrier creation and dynamics and surface trapping (photo part), as well as with phenomena associated with surface radicals formation and surface reactivity (catalysis part) [27]. There are recent experimental data of the authors published elsewhere on structure characterization and photocatalytic activity of the prepared nanocrystals with {0 0 1} dominated facets [28]. Photoconductivity measurement technique is a useful tool for the straightforward interpretation of the competition between photogeneration, recombination and trapping. Based on the literature review up to now, although widespread applications of TiO2 are credited to its high level of photoconductivity [29], no research effort has been devoted to the photoconductivity behavior of anatase TiO_2 nanoplates with {0 0 1} facets. The aim of the present work is to study the structural and transient photoconductive properties of anatase TiO2 nanoplates with dominant {0 0 1} facets and discuss the influence of the environment and calcining temperature.

2. Experimental details

2.1. Preparation of TiO_2 nanoplates

The samples were prepared using a solvothermal method. In a typical synthesis for TiO2 anatase nanoplates, 3 mmol of titanium isopropoxide [$Ti(C_3H_7O)_4$] from Alfa Aesar Chemicals was dissolved into 50 ml of absolute ethanol from Merck under vigorous stirring at room temperature. An amount of 0.6 ml (0.03 mol) hydrofluoric acid (HF 40%) from Merck was added into the ethanol solution as a capping agent. Then

the solution was pored into a 60 ml Teflon-lined autoclave until 80% of the volume was filled and was placed into the oven for 24 h at 180 °C. The as-synthesized powder products were collected through centrifugation of the solutions and washed three times with distilled water and dried in a furnace at 70 °C overnight.

In order to study the influence of the calcining temperature, some of the dried samples were calcinated in static air in a Muffle furnace for 90 min at 600 °C with a ramping rate of 5 °C/min. During this thermal treatment the adsorbed fluoride atoms are removed from the {0 0 1} crystal facets of TiO_2 anatase nanoplates. The samples were then cooled to room temperature.

So, two kinds of samples were prepared. The first were as prepared TiO_2 anatase nanoplates with exposed {0 0 1} crystal facets and the second resulted after a calcination treatment of these nanoplates at 600 °C.

2.2. UV–Vis

UV–Vis diffuse reflectance spectra of all samples were obtained for the dry-pressed film samples using a UV–Vis spectrometer (UV-2100, Shimadzu, Japan) with an integrating sphere attachment for their reflectance in the wavelength range 200–900 nm. BaSO4 was used as a reflectance standard. The widths of the effective band gap of the samples were determined using the Kubelka–Munk phenomenological theory.

2.3. Photoconductivity measurements

The transient photoconductivity of the samples was measured in different ambient environment, in vacuum (10^{-4} Pa) and in air. For these measurements, both the as prepared and the calcinated powders, after their preparation, were pressed into disks, applying a pressure of 30 Bar. The disks were 0.7 mm thick, with a diameter of 10 mm. Coplanar silver electrodes, 7 mm long and with a distance between them 0.8 mm,

were vacuum deposited on the samples. A vacuum cryostat was used, while the temperature was adjusted by an Oxford ITC502S temperature controller. A constant bias voltage of 5 V was applied to the samples, since no deviation from linearity in current–voltage curves was observed in the voltage range 1–10 V. The light source was a 100 W (white light) Xenon lamp. A heat filter was used for the white light heat filtering. The light intensity on the samples was 240 W/m^2, which was measured by an Ophir PD300-BB Radiometer head. The light was switched on and off every 20 min and the photocurrent response during illumination and darkness was measured by a Keithley 6517A electrometer and recorded every 10 s. For the elimination of persisting effects of previous light exposure, before any measurements in vacuum or in air, the samples were annealed at 440 K for 90 min and then they were left to cool down slowly. After that, they were maintained in the dark for 24 h for the dark conductivity relaxation to a quasi equilibrium value.

3. Results and discussion

3.1. Crystalline structure, diffuse reflectance and absorbance spectra

3.1.1. XRD, TEM and XPS

From the XRD patterns, the as prepared and calcinated at 600 °C nanoplates were found to be only anatase containing no impurities that may have been caused by the remaining precursor used each time or by the formation of another phase such as rutile [30]. From the TEM micrographs of the samples, the side length of the as prepared nanoplates was found ~24 nm and their thickness ~4 nm while the side length for the calcinated nanoplates was ~33 nm and their thickness ~25 nm [30].

Direct evidence from XPS measurements showing the existence of F atoms in the as prepared TiO$_2$ samples and the absence of F atoms in the calcinated ones has been found in our previous publication [28].

3.1.2. UV–Vis

Fig. 1 shows the UV–Vis diffuse reflectance and absorbance spectra of the as prepared and the calcinated at 600 °C anatase TiO$_2$ nanoplates. As can be seen the reflectance of the as prepared samples is about 42% and after calcinations it increases to about 82%. The determination of the band gap of the powders was evaluated using the Kubelka–Munk method based on the diffuse reflectance spectra [31]. The $(F(R)*E)^{1/2}$ versus $E(eV)$ plots of the samples are presented in Fig. 1, where $F(R) = (1 − R)/2R$. As can be seen all samples absorb at 400 nm due to the band gap absorption of anatase TiO$_2$, which is ~3.2 eV. More specifically, the as prepared nanoplates have an energy gap at 3.14 eV and the calcinated ones at 3.18 eV, implying that the fluoride atoms that are adsorbed on the {0 0 1} crystal facets of the as prepared samples do not cause a band-gap narrowing.
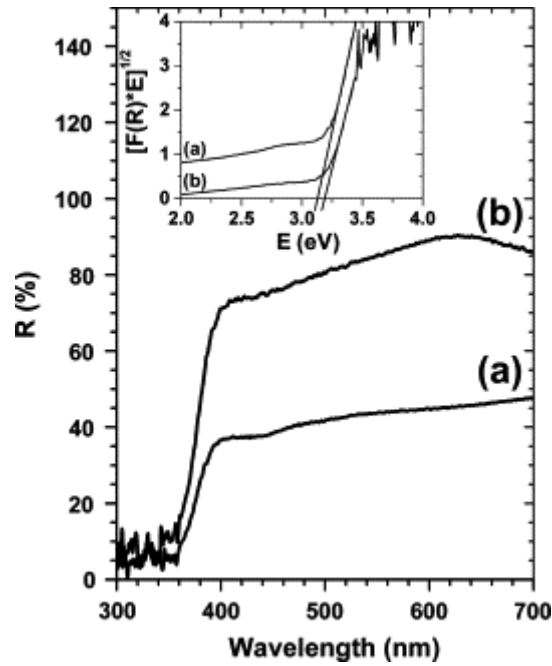
Fig. 1. UV–Vis diffuse reflectance spectra and in the inset the absorption spectra of the TiO$_2$ anatase nanopowders (a) as prepared, and (b) calcinated at 600 °C,

3.2. Transient photoconductivity measurements

3.2.1. In vacuum

The photoconductivity responses (σ_p) of the as prepared and the calcinated anatase TiO$_2$ nanoplates with dominant highly reactive {0 0 1} facets, in vacuum at 300 K, are illustrated in Figs. 2 and 3a, respectively. The dark conductivity values (σ_d) at 300 K, determined just before the onset of the illumination are 9.25×10^{-6} and 7.59×10^{-8} Ω^{-1} m^{-1} for the as prepared and the calcinated samples, respectively (Table 1). The difference of more than two orders of magnitude may be attributed to the fact that calcination treatment causes the escape of fluorine and in turn reduces the additional donor states and decreases electrical conductivity [32,33].
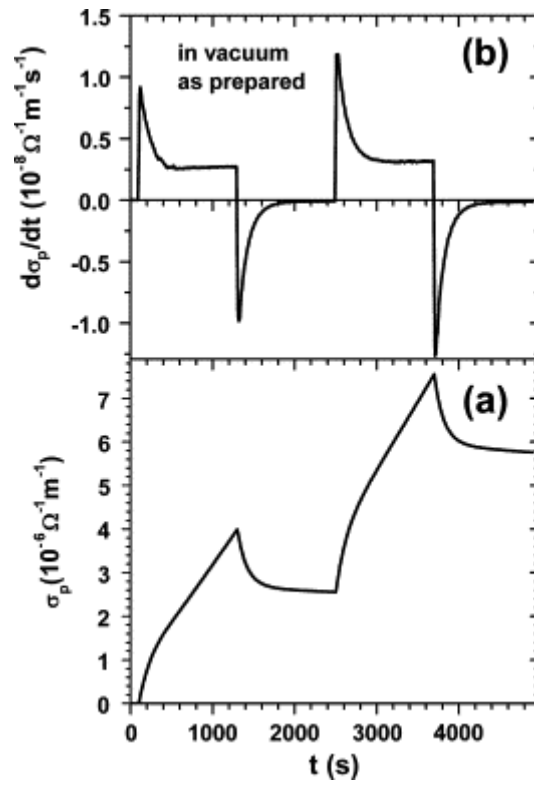
Fig. 2. The photoconductivity response (a), and the first derivative of the photoconductivity response (b), in vacuum at 300 K, of the as prepared TiO_2 anatase nanoplates.
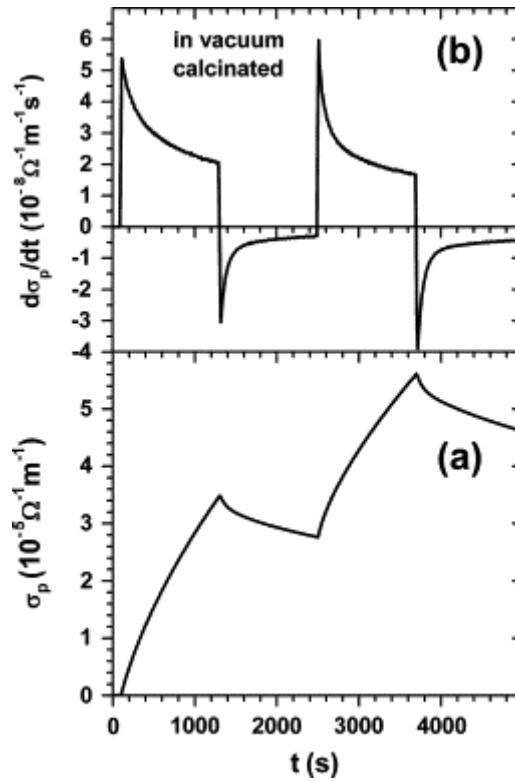
Fig. 3. The photoconductivity response (a), and the first derivative of the photoconductivity response (b), in vacuum at 300 K, of the calcinated at 600 °C TiO$_2$ anatase nanoplates.

Table 1.

Electrical conductivity σ_d and photoconductivity σ_p in vacuum and in air of the TiO$_2$ anatase nanopowders (a) as prepared, and (b) calcinated at 600 °C.

Samples	As prepared	Calcinated at 600 °C
In vacuum σ_d at 300 K (Ω^{-1} m^{-1})	9.25×10^{-6}	7.59×10^{-8}
In air σ_d at 300 K (Ω^{-1} m^{-1})	2.11×10^{-7}	5.86×10^{-10}
In vacuum σ_p after 20 min of illumination (Ω^{-1} m^{-1})	3.99×10^{-6}	$3.\,48 \times 10^{-5}$
In air σ_p after 20 min of illumination (Ω^{-1} m^{-1})	5.56×10^{-8}	6.61×10^{-9}

The σ_p values for both samples, at the end of the first illumination period, at 300 K, are given in Table 1. The calcinated sample presents a σ_p value about two and a half orders of magnitude larger than its dark conductivity and about an order of magnitude higher than the σ_p of the as prepared sample. For both samples, no saturation indication for the used light intensity appears, suggesting that even in vacuum some View the MathML source states remain on the surface.

The first derivatives $d\sigma_p/dt$ of the photoconductivity curves are shown in Fig. 2, Fig. 3b. At the early stages of illumination, $d\sigma_p/dt$ rises quickly reaching to a maximum which corresponds to the time needed for the quasi filling of the traps. Until then, the photogenerated electrons gradually fill the traps and the electron trapping rate decreases significantly resulting in a quick rise of photoconductivity. A high fall of $d\sigma_p/dt$ is shown immediately after the maximum, indicating that recombination becomes then important. The following decrease is slower due to the thermal electron release rate from the traps to the conduction band. In the case of the as prepared sample, after the first 540 s of illumination, $d\sigma_p/dt$ remains almost constant, indicating that thereafter the thermal release and recombination rates change with time in the same manner, resulting in a quasi linear trend of photoconductivity. The calcinated sample (Fig. 3b) shows a gradual decrease of $d\sigma_p/dt$ till the end of the first illumination period, giving to photoconductivity the usual sublinear behavior after the initial quick rise. The higher σ_p values are attributed to the thermal treatment which increases the crystallite size and in turn the crystalline quality enhances the amount of created excess charge carriers [27].

Just after the end of the first illumination period, $d\sigma_p/dt$ takes negative values for both samples, suggesting that the recombination rate then dominates and causes an initial abrupt fall in photoconductivity values. As time passes, the thermal release rate

becomes important resulting in a slower photoconductivity decrease. The slower decay of the calcinated sample, combined with its higher σ_p value at the onset of the decay period, implies its better crystallinity which enhances longer lifetimes and decreases the recombination rate [27]. The almost steady σ_p values of the as prepared sample, 500 s after the end of the first illumination period, suggests that the competing recombination and thermal release rates become then comparable.

The shown significant asymmetry between the two subsequent rises for both samples (Fig. 2, Fig. 3a), with σ_p reaching much higher values at the end of the second illumination period, originates from the fact that some traps remained filled even at the end of the first decay period [34, 35]. At the subsequent illumination, as fewer traps have to be filled, the photogenerated electrons are quickly activated to the conduction band. So a higher maximum value of $d\sigma_p/dt$ is achieved. As time passes, photoconductivity follows the same with the first illumination behavior. The ratio $\Delta\sigma_p/\sigma_{pa}$ takes the values 89% and 61% for the as prepared and the calcinated sample, respectively, where $\Delta\sigma_p$ is the difference between the σ_p values at the end of the second and first illumination respectively and σ_{pa} is the σ_p value at the end of the first illumination. In the case of the calcinated sample the ratio is lower, due to fact that $d\sigma_p/dt$ shows a more abrupt fall during the second illumination time, indicating that then recombination is more pronounced. The high σ_p value at the end of the decay time (more than two orders of magnitude larger than its dark value), combined with the creation of excess carriers under illumination, enhances recombination and causes a higher than the as prepared sample decrease in the σ_p value at the end of the second illumination period, as Fig. 3a shows.

3.2.2. In air

The σ_p behavior of the as prepared and the calcinated anatase TiO$_2$ nanoplates with dominant highly reactive {0 0 1} facets in air, at 300 K, is given in Figs. 4 and 5a, respectively. Their corresponding σ_d values at 300 K, just before the onset of illumination, are 2.11 × 10^{-7} and 5.86 × 10^{-10} Ω^{-1} m^{-1} and are listed in Table 1. They are significantly lower than those in vacuum attributed to the adsorbed oxygen gas molecules which capture electrons from the conduction band and the donor states to form O_2^- source [36]. The σ_p values in air after 20 min of illumination are presented in Table 1. A reduction in σ_p values about two and four orders of magnitude is observed in air for the as prepared and the calcinated samples, respectively, indicating that both samples are sensitive to the environment. Since the measurements are carried out in air, the pressure of oxygen is increased and the created by the adsorbed oxygen molecules great number of electron scavengers O_2^- source reduces the conduction electron density [35].
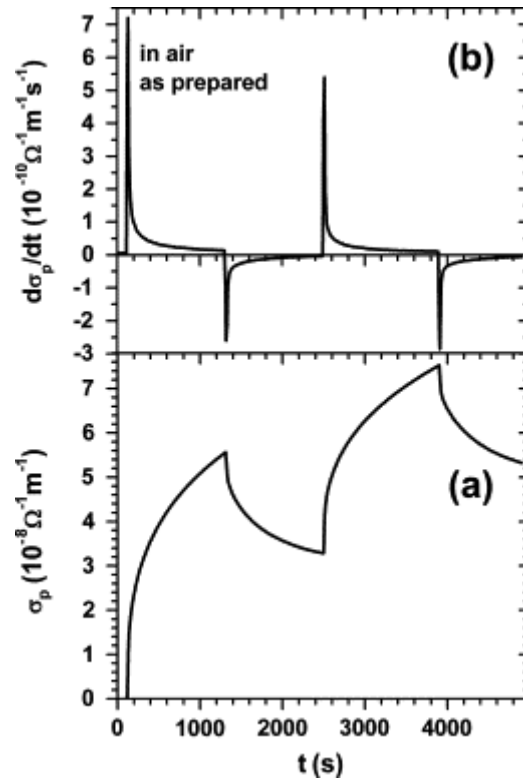
Fig. 4. The photoconductivity response (a), and the first derivative of the photoconductivity response (b), in air at 300 K, of the as prepared TiO_2 anatase nanoplates.
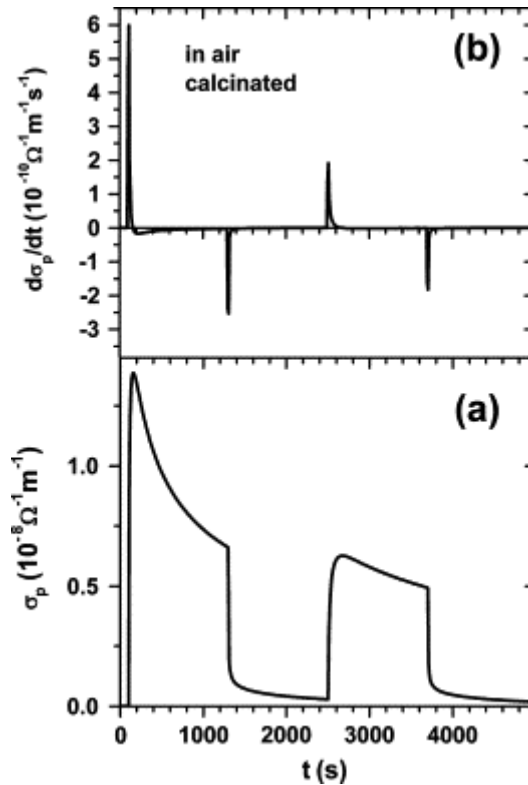
Fig. 5. The photoconductivity response (a), and the first derivative of the photoconductivity response (b), in air at 300 K, of the calcinated at 600 °C TiO$_2$ anatase nanoplates.

The $d\sigma_p/dt$ plots of the photoconductivity curves for the as prepared and the calcinated samples in air are shown in Figs. 4 and 5b respectively. In the case of the calcinated sample, $d\sigma_p/dt$ increases rapidly at the first stages of illumination taking a maximum value and then decreases quickly taking even negative values, suggesting the high domination of recombination in air. So the photoconductivity rises fast to a maximum and then decreases till the end of the illumination period (Fig. 5a), a well known behavior for TiO$_2$ samples in air [34,35,37]. At the end of the first illumination period, the σ_p has fallen to about 48% of its initial high value.

For the as prepared sample $d\sigma_p/dt$, after the initial maximum, does not take negative values till the end of the illumination period, indicating that thermal release rate is important. So, the σ_p behavior (Fig. 4a), compared to that of the calcinated sample, follows a quite different trend with time, showing no maximum and resembling to that in vacuum. Recombination is important for this sample in air, giving a more pronounced sublinearity in the curve, but it not so strong to cause the abrupt rise and the consequent fall of σ_p.

Immediately after the termination of illumination, $d\sigma_p/dt$ in air decreases highly to negative values for both samples, since the recombination rate then dominates. The created by thermal treatment trapping states act as recombination centers in air in the case of the calcinated sample. As time passes, the thermal release rate increases and thereafter $d\sigma_p/dt$ varies slowly. So, the photoconductivity falls abruptly at the early stages of the decay period and then a slow decrease follows. The σ_p decay of the as prepared sample is slower and resembles more to that in vacuum.

When the light is again turned on, $d\sigma_p/dt$ maximum values at the early stages of the second illumination are lower for both samples attributed to the high recombination rate in air. As Fig. 5a shows the σ_p of the calcinated sample initially reaches quickly a maximum value, 45% lower than the corresponding value at the first illumination period and then decreases slowly till the end of the second illumination period. Concerning to the as prepared sample (Fig. 4a), since transient photoconductivity has not taken its dark value at the end of the first decay, as it is expected, higher σ_p values are achieved.

4. Conclusions

In this work, the effect of thermal treatment as well as of environment on the transient photoconductivity behavior was investigated in anatase TiO_2 nanoplates with dominant {0 0 1} facets, prepared by a solvothermal method. Similar E_g values were found when fluorine atoms were adsorbed on the surface of TiO2 samples or when, because of heat treatment, they had escaped. The presence of fluorine increases the dark conductivity values in vacuum more than two orders of magnitude than those obtained after heat treatment.

The transient photoconductivity of the heat treated samples in vacuum reaches high values due to the enhancement of the amount of created excess charge carriers. The observed asymmetry between the subsequent rises is attributed to the fact that some traps remained filled even at the end of the first decay period.

Environment influences significantly conductivity as well as photoconductivity. In air, a decrease of several orders of magnitude in σ_p values may be ascribed to the created by the adsorbed oxygen molecules great number of electron scavengers O_2^-.

References

[1] U. Diebold, Appl. Phys. A 76 (2001) 1.

[2] M.R. Hoffmann, S.T. Martin, W. Choi, D.W. Bahnemann, Chem. Rev. 95 (1995) 69.

[3] A. Fujishima, T.N. Rao, D.A. Tryk, J. Photochem. Photobiol. C: Photochem. Rev. 1 (2000) 1.

[4] M. Asiltürk, F. Sayilkan, E. Arpac, J. Photochem. Photobiol. A 203 (2009) 64.

[5] G.Q. Wang, W. Lan, G.J. Han, Y. Wang, Q. Su, X.Q. Liu, J. Alloys Compd. 509 (2011) 4150.

[6] R. Asahi, T. Morikawa, T. Ohwaki, K. Aoki, Y. Taga, Science 293 (2001) 269.

[7] S. Bagwasi, Y. Niu, M. Nasir, B. Tian, J. Zhang, Appl. Surf. Sci. 264 (2013) 139.

[8] Y. Niu, M. Xing, J. Zhang, B. Tian, Catal. Today 201 (2013) 159.

[9] Y. Lv, L. Yu, H. Huang, H. Liu, Y. Feng, J. Alloys Compd. 488 (2009) 314.

[10] M. Iwase, K. Yamada, T. Kurisaki, O.O. Prieto-Mahaney, B. Ohtani, H. Wakita, Appl. Catal. B – Environ. 132–133 (2013) 39.

[11] G. Liu, L.Z. Wang, H.G. Yang, H.M. Cheng, G.Q. Lu, J. Mater. Chem. 20 (2010) 831.

[12] X.L. Hu, G.S. Li, J.C. Yu, Langmuir 26 (2010) 3031.

[13] J. Pan, G.Q. Lu, H.-M. Cheng, Angew. Chem. Int. Ed. 50 (2011) 2133.

[14] B. Zhang, J. Liu, S. Guan, Y. Wan, Y. Zhang, R. Chen, J. Alloys Compd. 439 (2007) 55.

[15] T. Sasaki, Y. Ebina, T. Tanaka, M. Harada, M. Watanabe, G. Decher, Chem. Mater. 13 (2001) 4661.

[16] H. Yu, B. Tian, J. Zhang, Chem. Eur. J. 17 (20) (2011) 5499.

[17] S. Liu, J. Yu, M. Jaroniec, Chem. Mater. 23 (2011) 4085.

[18] C.Z. Wen, H.B. Jiang, S.Z. Qiao, H.G. Yang, G.Q. Lu, J. Mat. Chem. 21 (2011) 7052.

[19] H.G. Yang, C.H. Sun, S.Z. Qiao, J. Zou, G. Liu, S.C. Smith, H.M. Cheng, G.Q. Lu, Nature 453 (2008) 638.

[20] Annabella Selloni, Nat. Mater. 7 (2008) 613.

[21] X. Li, J. Zhu, H. Li, Catal. Commun. 24 (2012) 20.

[22] K.P. Huber, G. Herzberg, Molecular structure IV constants of diatomic molecules, Van Nostrand Reinhold Company, New York, 1979.

[23] X. Han, Q. Kuang, M. Jin, Z. Xie, L. Zheng, J. Am. Chem. Soc. 131 (2009) 3152.

[24] X.H. Yang, Z. Li, G. Liu, J. Xing, C. Sun, H.G. Yang, C. Li, Cryst. Eng. Commun. 13 (2011) 1378.

[25] J.S. Chen, Y.L. Tan, C.M. Li, Y.L. Cheah, D. Luan, S. Madhavi, F.Y.C. Boey, L.A. Archer, X.W. Lou, J. Am. Chem. Soc. 132 (2010) 6124.

[26] W.Q. Fang, J.Z. Zhou, J. Liu, Z.G. Chen, C. Yang, C.H. Sun, G.R. Qian, J. Zou, S.Z. Qiao, H.G. Yang, Chem. Eur. J. 17 (2011) 1423.

[27] S. Boujday, F. Wünsch, P. Portes, J. Bocquet, Ch. Colbeau-Justin, Sol. Energy Mater. Sol. Cells 83 (2004) 421.

[28] M.V. Sofianou, C. Trapalis, V. Psyharis, N. Boukos, T. Vaimakis, J.G. Yu, W.G. Wang, Environ. Sci. Pollut. Res. 19 (2012) 3719.

[29] C.M. Teh, A.R. Mohamed, J. Alloys Compd. 509 (2011) 1648.

[30] K. Pomoni, M.V. Sofianou, T. Georgakopoulos, N. Boukos, C. Trapalis, J. Alloys Compd. 548 (2013) 194.

[31] E.L. Simmons, J. Mod. Optic. 19 (10) (1972) 845–851.

[32] X. Li, R. Xiong, G. Wei, Catal. Lett. 125 (2008) 104.

[33] P. Periyat, D.E. McCormack, S.J. Hinder, S.C. Pillai, J. Phys. Chem. C 113 (2009) 3246.

[34] K. Pomoni, A. Vomvas, Chr. Trapalis, Thin Solid Films 516 (2008) 1271.

[35] A.M. Eppler, I.M. Ballard, J. Nelson, Physica E 14 (2002) 197.

[36] N. Golego, S.A. Studenikin, M. Cocivera, Phys. Rev. B 61 (2000) 8262.

[37] S. Zhang, C. Xie, Z. Zou, L. Yang, H. Li, S. Zhang, J. Phys. Chem. C 116 (2012) 19673.